Regulatory variation controlling architectural pleiotropy in maize

Edoardo Bertolini[1], Brian R. Rice[2,a], Max Braud[1], Jiani Yang[1,b], Sarah Hake[3,4], Josh Strable[5], Alexander E. Lipka[2], Andrea L. Eveland[1,*]

[1]Donald Danforth Plant Science Center, St. Louis, MO 63132
[2]Department of Crop Sciences, University of Illinois, Urbana-Champaign, IL 61801
[3]Plant Gene Expression Center, USDA-ARS, Albany, CA 94710
[4]Plant and Microbial Biology Department, University of California, Berkeley, CA 94720
[5]Department of Molecular and Structural Biochemistry, North Carolina State University, Raleigh, NC 27695

*Corresponding author
[a]Current institution: Department of Agronomy and Horticulture, University of Nebraska-Lincoln, Lincoln, NE 68583
[b]Current institution: Bayer Crop Science, Chesterfield, MO 63107

Abstract

An early event in plant organogenesis is establishment of a boundary between the meristem and differentiating lateral organ. In maize (*Zea mays*), evidence suggests a common gene network functions at boundaries of distinct organs and contributes to pleiotropy between leaf angle and tassel branch number, two agronomic traits. To uncover regulatory variation at the nexus of these two traits, we used regulatory network topologies derived from specific developmental contexts to guide multivariate genome-wide association analyses. In addition to defining network plasticity around core pleiotropic loci, we identified new transcription factors that contribute to phenotypic variation in canopy architecture, and structural variation that contributes to *cis*-regulatory control of pleiotropy between tassel branching and leaf angle across maize diversity. Results demonstrate the power of informing statistical genetics with context-specific developmental networks to pinpoint pleiotropic loci and their *cis*-regulatory components, which can be used to fine-tune plant architecture for crop improvement.

34 Plant architecture has been an important target of selection in crop domestication and
35 improvement [1]. The domestication of maize from its wild progenitor teosinte involved major
36 architectural shifts in apical dominance and ear morphology that were pivotal in generating the
37 backbone of a highly productive crop [2]. Improvements to maize architecture through breeding
38 over the last century have substantially contributed to exponential yield gains; more compact
39 plants with upright leaves and smaller, fewer, or upright tassel branches enable increased
40 planting densities while enhancing photosynthetic efficiency in the lower canopy [3–6]. These
41 architectural traits are outputs of endogenous developmental programs, intricately connected
42 through gene networks that we are just beginning to unravel.
43 Variation in plant architecture typically involves changes in placement, number, or
44 orientation of lateral organs, which are initiated from populations of pluripotent stem cells called
45 meristems. Often, this is regulated by meristem determinacy programs [7] and the concept of
46 signaling centers acting in boundaries adjacent to meristems was proposed to modulate
47 meristem determinacy and architectural diversity [8]. During organogenesis, a boundary domain is
48 established between the meristem and differentiating lateral organs to restrict meristem
49 maintenance and organ identity genes to their respective zones [9]. Leaf angle (LA) in grasses is
50 largely determined by patterning and growth of the ligule and auricles, structures that
51 characteristically define the blade-sheath boundary and together act as a hinge to allow the leaf
52 to recline and absorb sunlight [9].
53 Several genes expressed at initiating ligules are also expressed at the boundaries of
54 other lateral organs, such as developing leaf primordia and tassel branches [10,11]. Among these
55 are *liguleless* (*lg*)*1* and *2*, which encode SQUAMOSA BINDING PROTEIN (SBP) and bZIP
56 transcription factor (TF)s, respectively. Loss-of-function mutants in these genes have
57 compromised ligule and auricle development, resulting in more upright leaves [12,13], but also
58 defects in tassel branch number (TBN) and angle (TBA) (Supplemental Note). Mutants in *lg2*
59 make few to no tassel branches that are upright compared to those of normal siblings [14], and *lg1*
60 has significantly fewer branches but the phenotype is less severe than in *lg2* [15]. Several other
61 maize mutants also show pleiotropic defects between leaf and tassel architecture traits,
62 including those with altered brassinosteroid (BR) signaling, a plant growth hormone that
63 modulates cell division and expansion [16,17] (Supplemental Note).
64 Core gene regulatory modules appear to underlie formation of a boundary, whether it is
65 the boundary at the ligule, the boundary between leaf primordium and meristem, or between
66 tassel branch and rachis. Similar to seminal findings in animal systems [18], these common
67 modules have likely been co-opted for development of distinct tissues and underlie pleiotropy

68 found between LA and TBN, important agronomic traits in maize improvement. Although
69 genome-wide association studies (GWAS) identified significant SNP-trait associations for TBN
70 in proximity to *lg1* and *lg2*, pleiotropy between these traits is less prominent in natural
71 populations [19]. This is likely due to regulatory variation within natural diversity, e.g., *cis*-
72 regulatory elements that specify spatiotemporal patterning of gene expression and are
73 hypothesized to be key drivers of phenotypic variation [20,21].
74 Pleiotropy, the effect of a gene on multiple phenotypic characters, is a major cause of
75 evolutionary constraint, and regulatory variation in pleiotropic loci underpins adaptive evolution
76 and developmental plasticity. Looking forward, the success of new technologies that allow
77 precise engineering of genomes and pathways will depend on our understanding of pleiotropy in
78 gene networks and devising ways of dissociating pleiotropic effects during crop improvement
79 [22,23]. The pleiotropy that exists between LA and TBN in maize, and the mutants that provide a
80 genetic framework for linking these traits, make it an ideal system for dissecting control points in
81 context-specific gene regulation. Here, we leverage this system and a novel approach that
82 integrates developmental biology, network graph theory and quantitative genetics to identify
83 new factors and regulatory variation that contribute to pleiotropy in tassel and leaf architecture.
84

85 **Results**

86 **A transcriptional framework for molecular explorations of tassel branching and leaf angle**

87 To delineate the gene networks underlying tassel branching and ligule development, and tissue-
88 specific rewiring around pleiotropic loci, we leveraged a panel of maize mutants with
89 developmental defects in TBN, LA or both, all well-introgressed into the B73 genetic background
90 (Fig. 1a). Mutants with altered TBN and/or TBA are described in the Supplemental Note and
91 include: *lg1*, *lg2*, *wavy auricle on blade1* (*wab1*) and the dominant *Wab1-R* allele, *ramosa1*
92 (*ra1*), *ra2*, *brassinosteroid insensitive1* (*bri1*)-*RNAi* and *bin2-RNAi*. These genetic stocks,
93 including B73 control plants, were grown in environmentally-controlled chambers to enable
94 precise developmental staging of different genotypes. Immature tassel primordia were hand-
95 dissected immediately before and after primary branch initiation (stage 1 and 2, respectively;
96 Supplementary Fig. 1). We also sampled across a five-stage developmental trajectory from
97 normal B73 tassels; the additional 3 stages representing different meristem transitions after
98 primary branch initiation. Mutants with defects in LA included *lg1*, *lg2*, *Wab1-R*, *bri1-RNAi*, *bin2-*
99 *RNAi*, and *feminized upright narrow* (*fun*), which makes a ligule but no auricles (Supplemental
100 Note). We sampled two sections of vegetative shoot from these mutants and B73 controls,
101 which we refer to as shoot apex 1 and 2: shoot apex 1 includes the shoot apical meristem

102 (SAM) and cells that are pre-patterned to be ligule, and shoot apex 2 was taken above the
103 meristem to include leaf primordia with developed ligules (Supplementary Fig. 1).
104 RNA-seq was used to profile gene expression across 140 samples (Supplementary
105 Table 1). Principal component analysis (PCA) of the normal B73 samples showed clear
106 separation by tissue type and mutant samples cleanly separated by genotype and tissue,
107 indicating distinct transcriptome profiles (Supplementary Fig. 2). Samples across the five stages
108 of B73 tassel development plotted in PCA space revealed a continuous transcriptional gradient
109 reflecting progression through specific axillary meristem types and progression from
110 indeterminate to determinate states. We first examined early shifts in gene expression during
111 primary branch initiation and leaf differentiation in normal B73 plants, which included genes
112 related to meristem identity and determinacy, organ specification, and growth hormone activity
113 (Fig. 1b and Supplementary Fig. 3). We tested for enrichment of functional categories using
114 Gene Ontologies (GO) within differentially expressed (DE) gene sets that were either up- or
115 down-regulated during the shift from meristem to organ differentiation, i.e., between stage 1 and
116 2 tassels (1,719) and shoot apex 1 and 2 (1,858) (Fig. 1b, Supplementary Tables 2 and 3). As
117 expected, enrichment of several GO categories shifted in common during tassel branch and
118 ligule development, e.g., those related to meristem activity and determinacy and inflorescence
119 morphogenesis, consistent with common sets of genes recruited for boundary establishment
120 and organ development. GO terms related to leaf morphogenesis showed opposite expression
121 between tissues, consistent with the leaf development program being suppressed during tassel
122 branch outgrowth (Fig. 1b). Several plant hormone pathways were overrepresented and tended
123 to show different trends during tassel branch and ligule development. For example, auxin and
124 BR genes showed common expression trajectories in the two developmental programs,
125 whereas jasmonic acid (JA), salicylic acid (SA) and particularly gibberellic acid (GA), showed
126 opposite trends (Fig. 1b). Members of certain developmental TF families showed specific
127 patterns of overrepresentation in tassel branching and leaf development (Supplementary Table
128 4 and 5). For example, ZINC FINGER HOMEODOMAIN (ZHD) and GRAS family TFs were
129 overrepresented during ligule development, several of which were annotated with GO terms
130 related to GA signaling (Supplementary Fig. 4).
131
132 **Heterochronic shifts in gene expression underlie tassel mutant phenotypes**
133 Along the defined expression trajectory of the B73 tassel, we interpolated the mutant tassel
134 expression data to capture deviations from this trajectory, i.e., shifts in heterochrony. We fit a
135 smooth spline regression model using expression values of the 500 most dynamically

136 expressed genes across normal tassel development and used this model to classify samples
137 relative to their transcriptomes, measured in expression time (ET) units (Fig. 1c). Expression
138 profiles of known marker genes in maize inflorescence development (e.g., meristem identity
139 genes) strongly support the ET classifications (Supplementary Fig. 5). Mutant expression data
140 showed clear shifts from normal tassel branch initiation and development, although phenotypic
141 differences were largely not observed at these stages (Fig. 1c). For example, ET classifications
142 of BR signaling mutants, *bri1*-RNAi and *bin2*-RNAi, were notably shifted compared to controls at
143 stage 1 but not stage 2. One interpretation is that transcriptional events modulated by BR
144 signaling during tassel development occur early at branch initiation and become more similar to
145 controls during branch outgrowth. The *bri1* and *bin2* genes encode positive and negative
146 regulators of BR signaling, respectively, and the RNAi mutants display opposite phenotypes for
147 LA and TBA (Fig. 1a; Supplemental Note). BRs play an important role in maintaining boundary
148 domain identity through control of cell division [24,25], which is consistent with strong shifts in BR
149 mutant gene expression as boundaries are developed during primary branch initiation.
150 Shifts in gene expression between tassel primordia at stages 1 and 2 were compared
151 between normal B73 controls and the two BR signaling mutants. Of 3,229 DE genes that
152 showed a differential expression trajectory in both mutants compared to controls, 2,235 showed
153 a larger difference at stage 1 (Fig. 1d, Supplementary Fig. 6). These latter DE genes were
154 enriched for functions related to both meristem maintenance and identity, consistent with
155 important boundary functions, and GA biosynthesis and signaling, suggesting cross-talk
156 between BR and GA pathways (Fig. 1e). Developmentally dynamic genes that were expressed
157 higher in BR signaling mutants at stage 1 were also significantly enriched for ZHD TF family
158 members (q = 2.45^{e-03}) (Fig. 1f; Supplementary Tables 6, 7, and 8). Notably, we observed
159 significant enrichment (q = 1.87^{e-02}) of SBP TFs among genes up-regulated in *bin2*-RNAi
160 mutants only during primary branch initiation when compared to normal plants, several of which
161 have been implicated in grass inflorescence development (Fig. 1f) [26,27].
162
163 **Gene network plasticity around pleiotropic loci in different developmental contexts**
164 To determine transcriptional hierarchies during tassel branch and ligule development we
165 integrated the expression data into 'tassel' and 'leaf' gene co-expression networks (GCNs) and
166 gene regulatory networks (GRNs). A common set of 22,000 expressed genes was used to
167 generate the two GCNs by weighted gene co-expression network analysis (WGCNA) [28]. Genes
168 were grouped based on their similar expression patterns into sixteen and eighteen co-

169 expressed modules in ‘tassel’ and ‘leaf’ networks, respectively, which are indicated by color
170 (Supplementary Fig. 7 and Supplementary Tables 9, 10).
171 To assess the extent of module conservation between the two GCNs, we conducted a
172 co-expression module preservation analysis based on a permutation method (n = 1,000;
173 Methods). We found that 11,221 nodes (52% of the commonly expressed genes) were
174 statistically preserved (α = 0.05, Fisher's exact test) and that 69% of the ‘tassel’ modules were
175 conserved with one or more sub-modules in the ‘leaf’ GCN (Fig. 2a and Supplementary Table
176 11). Two ‘tassel’ GCN modules (“brown” and “blue”) were the most preserved with more than
177 80% module conservation. The ‘tassel’ “brown” module included overrepresented genes
178 associated with regulation of meristem growth (GO:0010075, q = 7.74 e^{-05}) and maintenance of
179 shoot apical meristem identity (GO:0010492, q = 0.0035) (Supplementary Table 12). GO
180 enrichment analysis was performed on conserved ‘tassel-leaf’ GCN sub-modules
181 (Supplementary Table 13). For example, the ‘tassel’ “brown” GCN module included two
182 conserved sub-modules in the ‘leaf’ GCN; i.e., a ‘leaf’ “green” sub-module (nodes = 176,
183 Fisher's exact test P = 5.83 e^{-13}) and a ‘leaf’ “red” sub-module (nodes = 591, Fisher's exact test
184 P = 0) that were enriched for genes involved in GA (GO:0009740, q= 5.85 e^{-05}) and BR
185 (GO:0009742, q= 0.03) mediated signaling pathways, respectively.
186 To visualize network rewiring within preserved sub-modules, we conducted a
187 complementary GRN analysis to infer edge directionality. By overlaying the network connections
188 from the GCN and GRN, we observed that several highly-connected regulatory TFs had
189 conserved network connections in ‘tassel’ and ‘leaf’ networks. For example, ZHD15
190 (Zm00001d003645) showed a high degree of edge conservation in the “brown-green” sub-
191 module suggesting it is a conserved hub gene (Fig. 2b). The TF encoded by *knotted1* (*kn1*), a
192 master regulator of meristem maintenance including regulation of GA pathways [29], was also
193 predicted as a conserved hub. In contrast, the uncharacterized TF DOF25 (Zm00001d034163)
194 is potentially a transient hub connected to many genes in the ‘leaf’ GCN (*degree centrality* = 1)
195 but fewer in the ‘tassel’ GCN (*degree centrality* = 0.57).
196 Since *lg2* mutants are strongly pleiotropic for TBN and LA phenotypes, we investigated
197 tissue-specific connectivity of *lg2* in ‘tassel’ and ‘leaf’ GRNs. We observed substantial rewiring
198 of its closest neighbor nodes with a small degree of edge preservation between ‘tassel’ and
199 ‘leaf’, which included directed edges to *lg2* from TFs EREB92 (Zm00001d000339) and ABI41
200 (Zm00001d023446) (Fig. 2c). In the ‘tassel’ GRN, *lg2* was co-expressed with and co-regulated
201 by several different TFs including *tassel sheath4* (*tsh4*), an interaction that was validated
202 experimentally [30]. In the ‘leaf’ GRN, predicted regulators of *lg2* were significantly enriched for

203 HOMEOBOX (HB) (q = 1.3e^{-04}) and YABBY TFs (q = 2.38e^{-03}) (Supplementary Table 14), and
204 *lg2* was co-expressed not only with *lg1*, but also *liguleless related sequence1* (*lrs1*) and *sister of*
205 *liguleless1*, closely related paralogs of *lg2* and *lg1*, respectively. Prior work investigating
206 transcriptional networks at the blade-sheath boundary in maize similarly showed co-expression
207 among these genes [31].
208
209 **Network motif analysis resolves context-specific topologies and core regulatory factors**
210 To investigate the topology of the GRNs and interconnectedness of TFs, we annotated three-
211 node network motifs; simple, recurrent regulatory circuits that appear in the network at higher
212 frequency than expected by chance [32]. We used information derived from directed edges
213 inferred in the GRNs and systematically searched for three-node motifs (characterized by at
214 least three edges) that were significantly over-represented in the 'tassel' and 'leaf' GRNs. Out of
215 ten possible three-node motifs, three types were significantly enriched in both networks (Z score
216 > 20) and were present at a higher concentration (≥ 10%), namely the mutual-out, regulating-
217 mutual and feed-forward loop (FFL) (Fig. 3a and Supplementary Table 15). To determine which
218 TFs were predicted to be most influential in the transcriptional circuits, we ranked them based
219 on frequency within annotated three-node motifs. We selected the top one hundred recurrent
220 TFs from each of the 'tassel' and 'leaf' GCNs (Fig. 3b) for use in subsetting GWAS SNPs
221 (described below). TFs belonging to ZHD (q= 0.0028) and HB (q= 0.0002) families were the
222 most overrepresented in 'tassel' and 'leaf' GCNs, respectively.
223 FFLs have been described across organisms as local, repeated and adapted genetic
224 circuits [33]. To gain insight into the modularity of the FFLs within our context-specific GCNs, we
225 identified the overrepresented TFs in the two parallel regulation paths controlled by nodes "X"
226 and "Y" (Fig. 3c). GRAS, ZHD and SBP were the most overrepresented TF families in the
227 'tassel' $FFL_{(X)}$ while HBs were overrepresented in the 'leaf' $FFL_{(X)}$. In both networks, these TFs
228 were predicted to regulate several genes related to hormone biosynthesis and signaling and
229 nutrient sensing.
230
231 **A genomic selection approach to optimize phenotyping of maize diversity for**
232 **architectural pleiotropy**
233 We took a quantitative approach to identify loci that link TBN and LA in maize. To optimize
234 selection for maximizing diversity in these architecture traits, a genomic best linear unbiased
235 predictions model (GBLUP) was fit using the Goodman-Buckler diversity panel [34] and the
236 predicted genomic estimated breeding values (GEBVs) for the following traits in 2,534 diverse

237 lines from the Ames inbred panel [35]: TBN, LA, ear row number (ERN; included to maximize
238 diversity for ear traits too), and first and second Principal Components of the phenotypes
239 (PhPC1 and PhPC2, respectively) (Supplementary Table 16). Ames lines (*n*=1,064) were
240 randomly selected to represent the distribution of the predicted PhPC1 and manually
241 phenotyped for TBN and LA. Overall, the large portion of heritable variation among the selected
242 genotypes resulted in prediction accuracies of 0.58 and 0.50 for TBN and LA, respectively.
243 PhPC1 of the selected lines explained 56% of the total variance of TBN and LA, and was
244 explained by trait loadings that were both positive. PhPC2 explained the remaining variance
245 (44%) with positive (LA) and negative (TBN) loadings (Fig. 4a). Interestingly, PhPC1 explained
246 a larger portion of the variance than either TBN or LA, suggesting that PhPC1 may be a better
247 source for detecting pleiotropy than testing phenotypes independently.
248 Because plant architecture has played a key role in maize adaptation, we hypothesized
249 that genes underlying inflorescence and leaf architecture traits would be confounded with
250 population structure. This hypothesis was underscored by how clearly the proxy traits PhPC1
251 and PhPC2 subdivided the lines into their respective subpopulations (Fig. 4a). Moreover, we
252 observed a moderate correlation (0.53) between the PhPC1 (Supplementary Table 17) and
253 published flowering time data [36]. These results collectively suggest divergence between TBN,
254 LA, and their pleiotropic regulation across maize subpopulations. Thus, the models we used in
255 the ensuing analysis corrected for both population structure and familial relatedness (Methods).
256
257 **Network-assisted multi-trait GWAS identifies genetic loci associated with TBN and LA**
258 SNP markers were prioritized using gene sets related to TBN and LA based on network
259 analyses (described below) and were used to guide multivariate GWAS. While this approach
260 significantly reduced the marker density to varying degrees, we hypothesized that biological
261 information derived from the networks could resolve novel SNP-trait associated markers.
262 To select genes for marker sub-setting, we generated a comprehensive GCN using the
263 entire RNA-seq dataset (*n*=140) and identified sixteen modules of co-expressed genes. Using a
264 module-feature relationship analysis in WGCNA, we identified modules that had significant
265 correlations with tissue types, developmental stages or agronomic traits (Fig. 4b and
266 Supplementary Table 18). For each GCN module, we estimated TBN and LA narrow-sense
267 heritability (h^2) and compared the observed values to empirical distributions. Modules that fit the
268 following three conditions were selected (*n*= 6): i) significant module-trait correlation, ii)
269 observed h^2 values greater than the mean of their respective empirical distribution and iii) at
270 least 80% of genome-wide h^2 explained (Fig. 4b and Supplementary Table 19). SNPs

271 overlapping with genes in the selected six co-expression modules (*n*=106,790; within 2 kb
272 upstream and downstream of the gene model) accounted for nearly all of the genome-wide h^2
273 associated with TBN and LA (Supplementary Fig. 8). In addition to the combined GCN, we also
274 used a reductionist approach by selecting the top one hundred recurrent TFs within the three-
275 node network motifs derived from the 'tassel' and 'leaf' GRNs (Fig. 3b) as an alternative way to
276 partition SNP markers. Remarkably, SNPs (*n*=1,972) overlapping this group of genes still
277 explained a significant portion of the genome-wide h^2, 57% and 70% respectively for TBN and
278 LA (Supplementary Fig. 8).
279 For each set of markers, from 1) combined GCN and 2) three-node motif analysis, we
280 conducted single-trait GWAS for TBN, LA, and the first two PhPCs, and multi-trait GWAS
281 analyses for TBN and LA. Our GWAS models collectively yielded 71 and 172 non-overlapping
282 single trait-associated SNPs for the combined GCN and three-node motif sets, respectively
283 (Supplementary Table 20). The majority (72%) of the trait-associated markers in the three-node
284 motif set were associated with PhPC2, which represents opposite trait loadings. Genes
285 associated with PhPC2 were significantly enriched with GO terms implicated in meristem
286 determinacy and maintenance (Supplementary Table 21).
287 Multivariate analysis with the two marker sets identified a total of 23 potential pleiotropic
288 loci where SNPs simultaneously associated with both TBN and LA phenotypes (Fig. 4c and
289 Supplementary Table 22). Two of these SNPs were common in analyses with both marker sets
290 indicating high-confidence associations that may contribute to phenotypic pleiotropy. Both SNPs
291 were located within genes encoding TFs; one in the last exon of *ereb184* (Zm00001d034204),
292 an ortholog of *AINTEGUMENTA1* in *Arabidopsis thaliana* known to control plant growth and
293 floral organogenesis [37], and one in the last exon of *zhd21* (Zm00001d041780), which was
294 shown to express in leaf primordia during ligule initiation [31]. These two markers were also
295 associated with TBN in the single-trait GWAS. Also, the marker in *ereb184* associated with
296 PhPC1 in the single-trait GWAS, reinforcing the notion that PhPC1 may be used to detect
297 pleiotropic loci.
298 We found that *ereb184* and *zhd21* were connected in the 'leaf' GRN through four TFs:
299 *ereb93*, *zhd20, zhd16* and *barren inflorescence2;* the latter regulates tassel branch outgrowth in
300 maize [38]. Predicted downstream targets of these two TFs suggest that they regulate architecture
301 traits through different but interconnected developmental circuits made of several other *zhd*
302 genes, *knox* genes and genes regulating hormone metabolism, transport and signaling,
303 especially in auxin, GA and BR pathways (Fig. 4d and Supplementary Table 23). The link
304 between *ereb184* and *zhd21* was also supported by statistical epistasis analysis

305 (Supplementary Fig. 9 and Supplementary Table 24), which highlighted their interaction
306 together with other TFs and members of the ZHD family, such as *zhd1, zhd12 and zhd15*.
307
308 **Maize network data guide explorations of SNP-trait associations in sorghum**
309 We further tested whether the small set of markers selected based on three-node network
310 motifs in maize was sufficient to guide GWAS to candidate SNP-trait associations for LA in
311 sorghum. Among the maize genes within the motif set, we identified 146 sorghum orthologs and
312 their associated SNPs from the Sorghum Association Panel (SAP) [39]. Using the selected SNP
313 markers together with publicly available LA phenotype data for the SAP [40], we first tested h^2 for
314 this trait and found that variation in these genes explained more than 60% of the sorghum
315 genome-wide LA h^2 (Fig. 5a). Therefore, we conducted a single-trait GWAS for LA. Eight
316 sorghum LA-associated markers were found within or proximal to seven genes (Fig. 5b and
317 Supplementary Table 25), including orthologs of maize genes *nac112* (Sobic.009G143700),
318 *ofp39* (Sobic.008G042200), *c3h16* (Sobic.006G256500) and Zm00001d026535
319 (Sobic.006G254500), which were also identified in maize single-trait GWAS for PhPC1, PhPC2
320 and/or TBN. Additionally, a significant SNP was identified within the maize ortholog of *ereb114*
321 (Sobic.002G022600), a paralog of *ereb184*. Based on first neighbors' connectivity in the maize
322 'leaf' GRN, *ereb114* is situated either up- or downstream of known *knox* genes involved in
323 meristem maintenance and axillary meristem formation in maize, e.g., *kn1*, *gn1*, *rs1* and *lg4*,
324 suggesting conservation of developmental circuits controlling LA between maize and sorghum
325 (Fig. 5c). Furthermore, *ereb114* is predicted to directly target *zhd21*, another high-confidence
326 gene candidate from the multi-trait GWAS for LA and TBN.
327
328 ***zhd* genes modulate tassel and leaf architecture**
329 Throughout this study, genes encoding ZHD TFs repeatedly emerged as important players in
330 tassel branch and ligule development. These TFs appear as putative hubs in the networks or
331 highly connected to known developmental pathways. *Zhd* genes are enriched within BR
332 signaling-responsive genes during early development, and *zhd21* was identified as a high-
333 confidence candidate gene in multi-trait GWAS for TBN and LA. The extensive
334 interconnectedness among numerous ZHD family members suggests functional redundancy
335 and potential for molecular fine-tuning. To test whether disruption of network candidate *zhd*
336 genes have a phenotypic effect on tassel and/or leaf architecture, we studied the effects of
337 independent *Mutator* (*Mu*) transposon insertions in the coding regions of *zhd21* and *zhd1*
338 (UniformMu, Methods). One allele of *zhd21* (*zhd21-1*; mu1056071) showed significantly fewer

339 tassel branches and a more upright LA compared to W22 normal plants (Wilcoxon *p*-value
340 TBN=2.1e^{-04}, LA=8.5e^{-09}), while a different allele of *zhd21* (*zhd21-2*; mu1018735) and *zhd1*
341 (mu1022277) showed no significant difference in either trait (Fig. 6a). The mutation in *zhd21-1*
342 disrupts the zinc-finger domain, which we expect confers the observable phenotype. Since we
343 hypothesize some degree of functional redundancy among *zhd* genes, lack of phenotypes for
344 the other alleles was not surprising.
345 We tested whether stacking *zhd21* and *zhd1* alleles with no apparent phenotypes in
346 homozygous single mutants resulted in architectural differences. Interestingly, plants that were
347 homozygous for the *zhd1* mutant allele and heterozygous for *zhd21-2* had significantly more
348 tassel branches and more upright LA compared to plants heterozygous for both alleles
349 (Wilcoxon *p*-value TBN= 0.0094, LA= 0.0008) (Fig. 6b,c). Plants homozygous for *zhd21-2* and
350 heterozygous for *zhd1* showed no significant difference in either trait. Our results suggest that
351 *zhd21* and *zhd1* influence tassel branching and leaf architecture, and that complex network
352 connectivity among *zhd* family members may allow for precise modulation of pleiotropy in these
353 traits through combinations of alleles.
354
355 **Structural variation in the promoter of *ereb184* modulates pleiotropy in TBN and LA**
356 Our gene candidate *ereb184* was among the top hundred recurring TFs within 'leaf' GRN three-
357 node motifs and positioned as a regulatory factor in many FFLs ($FFL_{(x)}$; n=7,422). Notably,
358 these FFLs were overrepresented by ZHDs at the $FFL_{(y)}$ node (Fig. 7a). We found that *ereb184*-
359 regulated FFLs potentially regulate a set of downstream genes ($FFL_{(z)}$) associated with
360 functional categories that overlapped with those enriched during tassel branch and ligule
361 development (Fig. 7a and Supplementary Table 26). For example, four KN1-regulated FFLs
362 (validated by ChIP-seq data [29]) included *ereb184* connections to several known homeotic genes
363 that were predicted in the 'leaf' GRN to directly target *lg2* (Fig. 7b).
364 Scanning the gene regulatory space around *ereb184,* we observed approximately 100
365 kb of intergenic sequence upstream of the TSS. We integrated publicly available omics'
366 datasets to investigate potential regulatory regions (see Data accessibility). We identified three
367 genomic regions with regulatory signatures including unmethylated marks, which colocalized
368 with conserved non-coding sequences and showed increased nucleotide diversity, similar to
369 that overlapping the coding region of *ereb184* (Fig. 7c). To investigate tissue-specific chromatin
370 accessibility, we generated Assay for Transposase-Accessible Chromatin (ATAC)-seq data from
371 the B73 shoot apex 2 tissue (including developed ligules) and compared the profiles in this
372 region to publicly available ATAC-seq data from tassel primordia [41]. All three regulatory regions

373 showed tissue-specific chromatin signatures that overlapped with other epigenetic marks,
374 highlighting potential tissue-specific regulation of *ereb184*. Overlaying publicly available maize
375 leaf chromatin interaction data (Hi-C) [42] predicted chromatin looping between the *ereb184*
376 promoter and one of the upstream intergenic regions (Fig. 7c).
377 Using public data from the maize Nested Association Mapping (NAM) Consortium [43], we
378 identified structural variation (SV) of approximately 5 kb in the promoter region of *ereb184*.
379 Based on resequencing data of the 26 NAM founder lines, this SV was either present or absent,
380 and mainly absent in tropical inbred lines. We also observed tissue-specific chromatin
381 accessibility adjacent to the SV, suggesting it is located within a regulatory region. We tested
382 whether presence/absence variation (PAV) of the SV in the promoter of *ereb184* influenced
383 pleiotropy between TBN and LA. In addition to the NAM founder reference genomes, we
384 extended the analysis to include 231 accessions that we phenotyped from the Goodman-
385 Buckler panel [34], incorporating existing sequencing data [44] to define PAV. Strikingly, we found
386 that maize lines without the SV showed increased TBN and had more upright leaves, while lines
387 with the SV showed the opposite trend, and these results were significant by Wilcoxon rank-sum
388 test (p-values TBN= 0.0078, LA= 0.043) at $\alpha = 0.05$. Also, based on transcriptome data from the
389 NAM Consortium, founder lines with the SV present in the *ereb184* promoter had lower gene
390 expression (Wilcoxon rank-sum test p=0.029) in shoot tissue (Fig. 7c). These results show that
391 SV in the *ereb184* promoter contributes to regulation of these pleiotropic, agronomic traits.
392
393 **Discussion**
394 In maize, mutants that affect the ligule also affect tassel branch initiation and genes expressed
395 at initiating ligules are also expressed at the boundary of other lateral organs [10,11] such as tassel
396 branches. In this study, we leveraged this well-characterized maize genetics system to
397 investigate the molecular underpinnings of pleiotropy: network rewiring around pleiotropic
398 factors in two developmental contexts, the redeployment of TFs for analogous but different
399 developmental processes, and *cis*-regulatory variation modulating pleiotropic loci. By
400 strategically integrating context-specific biological data and multivariate GWAS models that
401 exploit maximal diversity in TBN and LA, we identified new regulatory factors contributing to
402 architectural pleiotropy in maize. Our approach can be applied in any genetic system to
403 disassociate pleiotropic phenotypes through manipulation of *cis*-regulatory components and
404 gene network connections.
405 Pleiotropy in crop phenotypes can limit productivity ceilings. For example, selection on a
406 certain desired phenotype may come with unintended deleterious manifestations of another.

407 This can happen when a gene controlling a target trait also functions in another developmental
408 or physiological context. In recent years, the dramatic production gains of the 20th century have
409 plateaued in the world's most important cereal crops [45]. Looking forward, step changes in crop
410 improvement and sustainability will rely on targeted manipulation of regulatory pathways to fine-
411 tune agronomic traits for enhanced plant productivity and resilience in dynamic environments
412 [46,47]. Central to this is the ability to predict and design highly-specific genetic changes at
413 pleiotropic loci with minimal perturbation to the complex networks in which they reside.
414 Therefore, knowledge of context-specific gene networks and functional *cis*-elements will enable
415 greater precision in engineering or breeding optimal plant ideotypes.
416 In comparing predicted gene regulatory interactions between tassel branch and ligule
417 development, both conservation and rewiring of the GRNs were observed. For example, KN1
418 and ZHD15 were maintained as hubs with conserved regulatory connections in both
419 developmental contexts. Conservation around KN1 was not unexpected given its role as a
420 master regulator of meristem maintenance. Identifying ZHD15 as a conserved hub was novel,
421 but consistent with several lines of evidence in this study that implicate ZHDs as central players
422 in architectural pleiotropy between tassel branching and leaf architecture. Alternatively, there
423 was extensive rewiring of predicted network connections around LG2, which strongly controls
424 TBN and LA in a pleiotropic manner. This suggests that re-deployment of LG2 in different
425 developmental contexts was likely accompanied by loss and gain of regulatory connections to
426 gene targets and targeting TFs. Perhaps LG2 serves a common function in setting up
427 boundaries and its interactions with context-specific sub-networks shape the specific
428 developmental programs.
429 We showed that these biological context-specific networks could be used to subset
430 markers for multi-trait GWAS and identify new loci that contribute to architectural pleiotropy in
431 TBN and LA. Using two different network-guided approaches we identified several gene
432 candidates in and around significant SNP-trait associations. Strikingly, both approaches
433 identified significant SNPs within two of the same TF-encoding genes, *zhd21* and *ereb184.* Both
434 TFs are members of large families that are largely uncharacterized in maize and our results
435 showed that *zhd* and *ereb* TFs were highly interconnected within the regulatory networks
436 controlling tassel and leaf architecture. Furthermore, stacking *zhd* alleles with no observable
437 phenotypes in these traits resulted in pleiotropic phenotypic expressions. This suggests
438 functional redundancy among *zhd* genes and that further analyses of genetic interactions
439 among *zhd* mutant alleles should provide insight into how to precisely manipulate plant
440 architecture.

The vast stretch of intergenic space (~100 kb) upstream of *ereb184* is sprinkled with regulatory signatures, including tissue-specific accessible chromatin regions, which potentially regulate its context-specific expression. The SV in its upstream promoter region, which is present in approximately half of the NAM founders, appears to control expression of *ereb184*; expression levels are significantly different in NAM lines with the SV compared to those that don't. Presence or absence of the SV may contribute to differences in spatiotemporal expression patterns of *ereb184* and underlie the shifts in pleiotropy between TBN and LA. The origin of this SV is unclear. A blast search of the SV DNA sequence against a curated transposable element database revealed the presence of a probable LTR Gypsy retrotransposon (86% alignment identity) in the 3-prime region of the SV, as well as interspersed Helitron fragments. Differential chromatin accessibility between tassel primordia and shoot apex was evident in a regulatory region immediately proximal to the SV. Perhaps the SV is disrupting TF-binding interactions in the *ereb184* promoter or even interfering with long-range regulation through chromatin looping as suggested by a proximal Hi-C interaction.

Small effect loci for target traits are difficult to pinpoint with GWAS given that large trait effects generally dominate, which is compounded by the threshold for significance rising with marker density due to multiple correction. Targeted GWAS with a limited, but biologically informed marker set, has been demonstrated using pathway enrichment analysis [48] and chromatin accessible regions [49]. Application of these methods to identify informative smaller SNP sets can enhance genomic predictions. Here, we showed that even SNP subsets identified with small numbers of genes prioritized through network analyses not only produced heritabilities similar to a genome-wide set of markers, but also enabled detection of small effect loci that were validated to contribute to both tassel and leaf architecture. Notably, we further showed that the context-specific networks from maize could be used to inform GWAS for LA in closely related sorghum. The analysis in sorghum identified *ereb114*, a paralog of *ereb184*, which was connected to it and *zhd21* in the network.

Our analyses support the utility of biologically informed, context-specific networks for guiding GWAS in various applications and for identifying loci that connect phenotypic traits. Results highlight various mechanisms by which expression of pleiotropic trait phenotypes are modulated, including through network interconnectedness of functionally redundant TF family members or SV in *cis*-regulatory components. We anticipate that this approach can be used widely to identify pleiotropic loci for manipulation in crop improvement.

475 **Figure legends**

476 **Fig. 1: Transcriptional analyses across maize mutants with defects in leaf angle and**
477 **tassel branching**

478 **a)** Panel of maize mutants used in this study depicting unique tassel branching phenotypes
479 compared to B73 controls. Color scale in the heatmap indicates severity of tassel branch
480 number (TBN), tassel branch angle (TBA) and leaf angle (LA) phenotype deviations from B73
481 controls; dark blue-to-white = strong-to-weak phenotype. **b)** Enrichment of GO terms associated
482 with DE gene sets identified during the shift from stage (stg) 1 to stg 2 tassel primordia and from
483 shoot apex 1 to shoot apex 2. **c)** A 2-dimensional section of the first and second PC from the
484 normal B73 tassel developmental gradient (n = 20). The blue line represents the b-spline fit with
485 three degrees of freedom modeled within the dataset and used to classify samples relative to
486 their developmental progression coded as expression time (ET). Colored squares represent the
487 20 tassel samples in ET. The dot plot below represents tassel primordia stgs 1 and 2 from the
488 different mutant backgrounds. Mutant data points are color-coded relative to B73 ET. Stages of
489 meristem development along normal tassel developmental time are indicated: inflorescence
490 meristem (IM), branch meristem (BM), spikelet pair meristem (SPM), spikelet meristem (SM). **d)**
491 Venn diagram shows genes that are DE in tassel primordia during shift from stg 1 to 2 and DE
492 in *bri1-RNAi* and *bin2-RNAi* mutants compared to B73 controls. Those with stronger deviations
493 at stg1 are shown in parentheses. The ternary plot below shows the relative expression of
494 genes commonly mis-expressed between the two mutants compared to B73 at stg 1. Each dot
495 represents a gene and its coordinates indicate relative expression in the three genotypes. Some
496 examples of classical maize genes are noted. **e)** The top heatmap shows GO terms enriched
497 among DE gene sets commonly expressed either higher or lower in the BR mutants compared
498 to B73 controls in stg 1 tassels (from the ternary plot in d); the bottom heatmap shows
499 overrepresented TF classes among genes expressed higher in *bri1* and *bin2* mutants at stg 1
500 and those expressed higher in *bin2* only compared to B73 controls. **f)** Relative gene expression
501 trends are shown for ZHD and SBP TF family members that were expressed higher in *bin2*
502 and/or *bri1* mutants compared to B73 controls at stg 1. Arrows indicate direction of expression
503 change between stg 1 and 2 tassel primordia.

504

505 **Fig. 2: Conserved and divergent network connections between tassel and leaf gene**
506 **regulatory networks**

507 **a)** Gene co-expression network (GCN) preservation between ‘tassel’ and ‘leaf’ networks.
508 Preserved modules are indicated by color and connected by lines (width is proportional to

509 number of preserved genes). Colored boxes beneath the plot represent example preserved
510 gene co-expression sub-modules. **b)** Topological graph representation of preserved TFs in the
511 'tassel'-'leaf' "brown-green" sub-module based on data from GCN (edge weight) and gene
512 regulatory network (GRN; edge directionality). Pink edges represent preserved regulatory
513 connections and brown or green edges represent the network-specific wires. **c)** Topological
514 graph representation of closest TF neighbors to *liguleless2* (*lg2*) in the 'tassel' and 'leaf'
515 networks based on data from GCN (edge weight) and GRN (edge directionality). Pink edges
516 represent preserved connections and blue or brown/green edges represent network-specific
517 wires. The edge length is proportional to the weight of gene co-expression. Nodes are colored
518 based on their GCN module designation. Maize gene labels are from MaizeGDB or AGPv4 as
519 $Zm00001d_{(6)}$.
520
521 **Fig. 3: Analysis of three-node network motifs**
522 **a)** The number and type of three-node motifs identified in 'tassel' and 'leaf' GRNs compared to
523 randomized networks (n = 1,000). The x-axis represents the motif type (from A to J) of three-
524 node motifs with edge number ≥ 3. **b)** Top 100 ranked TFs based on their occurrence in the
525 three-node motifs grouped by family. Bars represent TF frequency in the three-node motif (scale
526 in red is TF frequency / 10,000); non-normalized values are within parentheses. TF labels are
527 from MaizeGDB or AGPv4 as $Zm00001d_{(6)}$. **c)** Examples of feed-forward loop (FFL) motifs
528 mediated by select TFs. The heatmap displays overrepresented TFs in $FFL_{(X)}$, (examples of
529 genes in each TF family are noted). Nodes represent genes, while the directed edges represent
530 the potential regulatory relationships.
531
532 **Fig. 4: Multi-trait GWAS detected candidate pleiotropic genes for TBN and LA**
533 **a)** Phenotypic Principal Components (PhPCs) of TBN and LA. Individuals are plotted according
534 to their PhPC1 scores of TBN and LA on the x-axis and their PhPC2 scores on the y-axis. The
535 percentage of total variance explained by a component is listed in parentheses on the axis. Blue
536 arrows represent trait loadings for a given PhPC where its direction on the x-axis represents its
537 contribution to PhPC1 and direction on the y-axis, its contribution to PhPC2. Subpopulations are
538 color-coded and grouped according to PhPCs. **b)** Analysis of module-trait relationships for the
539 combined GCN. Modules are represented as colored boxes with the number of co-expressed
540 genes indicated. The correlogram to the right represents the module-trait relationship where
541 shades of blue and red represent positive and negative Pearson's correlation, respectively, with
542 darker colors indicating a stronger positive or negative correlation. Modules representing more

543 than 80% of the whole genome heritability (h^2) for TBN and LA are indicated. **c)** Multi-trait
544 GWAS results using subsets of markers within 2 kb proximity of genes in the six co-expression
545 modules with significant h^2 in panel b (top) and in the top 200 interconnected TFs within three-
546 node motifs from Fig. 3b. Brown and blue dots represent significant SNP-trait associations; blue
547 dots indicate loci identified in both analyses. **d)** Topological graph representation of a sub-
548 network including *ereb184*, *zhd21* and their predicted downstream target genes based on data
549 from the 'leaf' GRN (edge directionality).
550
551 **Fig. 5: GWAS for LA in sorghum using biological information derived from maize**
552 **a)** LA narrow-sense heritability of 146 sorghum-maize syntenic orthologs in comparison to a null
553 distribution (violin plot). Purple line represents 95% cut-off, red line represents LA h^2 of the
554 sorghum orthologs, green line is the whole genome LA h^2. **b)** Manhattan plot showing GWAS
555 results for LA based on markers in proximity of the 146 sorghum-maize syntenic orthologs.
556 Purple dots represent significant SNP-trait associations for LA. **c)** Topological graph
557 representation of *ereb114* and its closest network neighbors in the maize 'leaf' GCN (edge
558 weight) and GRN (edge directionality). Green and purple nodes and edges are colored based
559 on module assignment in the 'leaf' GCN. Pink edges represent preserved connections with the
560 'tassel' GCN. Edge length is proportional with the gene co-expression weight.
561
562 **Fig. 6: *zhd* mutant alleles contribute to tassel and leaf architecture**
563 **a**) Phenotypic characterization of TBN and LA in homozygous *zhd* alleles compared with w22
564 control plants. **b**) Representative tassel branch and leaf angle phenotypes resulting from genetic
565 interactions between mutant alleles of *zhd1* and *zhd21*, from left to right: *zhd1/*+;*zhd21-2/*+,
566 *zhd1/*+;*zhd21-2/zhd21-2*, *zhd1/1*;*zhd21-2/*+. Black bar = 1cm. **c)** Among combinations of mutant
567 alleles, *zhd1/1*;*zhd21-2/*+ showed significant differences in TBN and LA compared to
568 *zhd1/*+;*zhd21-2/*+ normal siblings based on Wilcoxon rank-sum test.
569
570 **Fig. 7: *ereb184* modulates pleiotropy in TBN and LA**
571 **a)** FFLs from the 'leaf' GRN are represented with *ereb184* in each of the node positions and
572 number of times each occurs. The graph below shows GO terms overrepresented within the Z
573 position when EREB184 is in the X position. **b)** An example of a sub-network from the 'leaf'
574 GRN shows *ereb184* participating in multiple FFLs with KN1 and other proximal-distal patterning
575 TFs that target *lg2*. The solid yellow arrows represent ChIP-seq validated connections. **c)**
576 Genomic view of the intergenic space upstream (100 kb) and just downstream of *ereb184*. The

577 tracks from top to bottom: nucleotide diversity (π), conserved non-coding sequences, multi-trait
578 GWAS, unmethylated regions, leaf chromatin interaction data (Hi-C), structural variation, RNA-
579 seq, and ATAC-seq. Data from public sources are indicated in Data Accessibility. **d)** The effect
580 of structural variation (SV) presence/absence in the promoter region of *ereb184* across 231
581 accessions on TBN and LA traits, and the effect of SV on *ereb184* expression within 26 NAM
582 founder lines.
583
584 **Supplementary Figure Legends**
585 **Supplementary Fig. 1: Overview of biological samples collected for this study**
586 Representative images of hand-dissected tassel primordia from B73 control plants at **A**. stage 1,
587 which captures branch meristem initiation and **B**. stage 2, which captures branch outgrowth.
588 Scale bars = 1,000 μm. **C**. Longitudinal section through the shoot apical meristem (SAM) of a
589 B73 control plant depicting the microscopic view of the shoot apex to the right. *In situ*
590 hybridization with a *liguleless1* (*lg1*) anti-sense probe marks developing ligules. Two sections
591 from the shoot apex were sampled: shoot apex 1 includes the SAM and cells pre-patterned to
592 be ligule and shoot apex 2 excludes the SAM and enriches for developed ligule. Leaf primordia
593 are designated according to plastochron number (P). White arrow denotes the pre-ligular band
594 while black arrows indicate the developing ligule on P7 and successive leaf primordia.
595
596 **Supplementary Fig. 2: Principal component analysis of the expression dataset**
597 The image shows the three principal components in 3-dimensional space of the entire
598 transcriptional dataset (*n*=140) generated from the two tassel primordia developmental stages
599 and shoot apex sections. Genotypes are marked by different colors and tissue type by different
600 symbols. The principal component analysis was calculated based on the top 500 dynamically
601 expressed protein-coding genes.
602
603 **Supplementary Fig. 3: Dynamically expressed genes during tassel branching and ligule**
604 **differentiation**
605 **A.** Volcano plot showing variation in gene expression associated with tassel branch
606 development based on comparing between tassel stages 1 and 2 in B73 normal plants. Genes
607 expressed higher in stage 2 are in blue and those in yellow are decreasing in expression. **B.**
608 Volcano plot representing variation in gene expression associated with ligule differentiation
609 based on the comparison between the shoot apex 1 and 2 samples in B73 normal plants.
610 Genes expressed higher in shoot apex 2 are in blue and those in yellow are decreasing in

611 expression. Only genes with FDR < 0.05 are plotted along the x- (log2 fold change) and y- (-
612 log10 FDR) axis. Some classical maize genes are annotated.
613
614 **Supplementary Fig. 4: Many genes are differentially expressed in two developmental**
615 **contexts during tassel branch outgrowth and ligule differentiation**
616 The heatmap displays relative gene expression profiles of annotated TFs and classical maize
617 genes across both stages of tassel primordia and shoot apices sampled (n = 86). Genes were
618 differentially expressed in the comparisons between tassel stages 1 and 2 and between shoot
619 apex 1 and 2 with FDR < 0.05 (gray area of the Venn diagram). For each developmental
620 context, DE genes that were up-regulated across developmental time are annotated with a blue
621 box and down-regulated genes annotated with a yellow box.
622
623 **Supplementary Fig. 5: Maize developmental marker genes correspond to meristem**
624 **identity and determinacy shifts across the tassel developmental gradient**
625 Expression trajectories of known maize developmental marker genes for meristem identity and
626 determinacy are visualized to assess robustness of the five stage B73 normal tassel
627 developmental gradient. **A**. Heatmap shows gene expression of selected maize inflorescence
628 markers across the five tassel primordia stages in B73. **B.** Peak expression of classical maize
629 genes associated with each stage of meristem development in B73 is shown on the left, and
630 expression profiles for these marker genes in *liguleless2* and *ramosa1* mutant backgrounds are
631 shown on the right. The *branched silkless1* profile is not shown in the mutants since it comes on
632 after stage 2.
633
634 **Supplementary Fig. 6: Differences in gene expression of BR mutants compared to B73**
635 **controls in stage 2 tassels**
636 The ternary plot shows the relative expression of genes mis-expressed in common between the
637 two BR mutants compared to B73 at stage 2. Each dot represents a gene and its coordinates
638 indicate relative expression in the three genotypes.
639
640 **Supplementary Fig 7: Eigengene trajectories of co-expression modules from 'tassel' and**
641 **'leaf' networks**
642 The expression profile that best fits an average of all genes within a co-expression module is
643 depicted as a Module Eigengene (ME). For each co-expression module in the **A.** 'tassel' and **B.**
644 'leaf' GCNs, MEs are depicted by dots in each sample. Each module showed a distinct

645 expression profile, with certain modules characterized by peak expression at specific
646 developmental stages and/or in certain mutant backgrounds.
647
648 **Supplementary Fig. 8: Density plots representing empirical distributions in comparison**
649 **to whole genome h^2 and TBN and LA h^2**
650 **A.** TBN h^2. Above 0 density represents the null distribution (purple arrow shows the 95th
651 percentile) in comparison to h^2 explained by the selected co-expressed network modules
652 (orange arrow) and whole genome h^2 (green arrow). Below 0 density represents null distribution
653 (purple arrow shows the 95th percentile) in comparison to h^2 explained by the combined
654 network motif (orange arrow) and whole genome h^2 (green arrow). B. LA h^2. Upper panel
655 represents the null distribution (purple arrow shows the 95th percentile) in comparison to h^2
656 explained by the selected co-expressed network modules (orange arrow) and whole genome h^2
657 (green arrow). Lower panel represents null distribution (purple arrow shows the 95th percentile)
658 in comparison to h^2 explained by the combined network motif (orange arrow) and whole genome
659 h^2 (green arrow)
660
661 **Supplementary Fig. 9: Depiction of statistical genetic interactions predicted for ereb184**
662 **with the top recurrent TFs within three-node network motifs**
663 Based on makers within the genomic windows defined as ± 2 kb from the transcriptional start
664 site (TSS) and transcriptional termination site (TTS) of *ereb184 and the recurrent TFs from 3-*
665 *node motifs*, statistical genetic interactions were predicted. These interactions are represented
666 as links between genes located on a circular visualization of the maize genome. Grey and tan
667 links represent significant interactions for the traits TBN, LA and PhPC2. Tan links highlight
668 statistical interactions that are supported by the GRN data.
669
670 **Supplementary Tables**
671 **Supplementary Table 1:** Gene expression in TPM across 140 RNA-seq samples.
672 **Supplementary Table 2:** DE genes with FDR < 5% derived from the comparison of B73 stage
673 2 tassel primordia vs. stage 1.
674 **Supplementary Table 3:** DE genes with FDR < 5% derived from the comparison of B73 shoot
675 apex 2 vs. shoot apex 1.
676 **Supplementary Table 4:** GO terms associated with DE genes derived from the comparison of
677 B73 stage 2 tassel primordia vs. stage 1.

678 **Supplementary Table 5:** GO terms associated with the DE genes derived from the comparison
679 of B73 shoot apex 2 vs. shoot apex 1.
680 **Supplementary Table 6:** Genes that are DE between tassel stage 1 and stage 2 and shared
681 between the BR mutants compared to B73 control.
682 **Supplementary Table 7:** Relative expression of genes commonly DE in the two BR mutants
683 along the tassel stage 1 to stage 2 developmental gradient compared to the B73 control.
684 **Supplementary Table 8:** GO and TF enrichment analysis of genes commonly DE in the two BR
685 mutants between tassel stage 1 and stage 2 development compared to the B73 control.
686 **Supplementary Table 9:** Summary of gene co-expression modules from the 'tassel' and 'leaf'
687 context-specific networks.
688 **Supplementary Table 10:** Maize genes grouped based on the 'tassel' and 'leaf' gene co-
689 expression modules.
690 **Supplementary Table 11:** Gene co-expression module preservation matrix between 'tassel'
691 and 'leaf' networks.
692 **Supplementary Table 12:** GO terms overrepresented within 'tassel' and 'leaf' GCN modules.
693 **Supplementary Table 13:** GO terms overrepresented within 'tassel' and 'leaf' GCN preserved
694 sub-modules.
695 **Supplementary Table 14:** TF enrichment analysis of the predicted regulators of *liguleless 2* in
696 the leaf GRN shown in Figure 2c.
697 **Supplementary Table 15**: i) Summary statistics of the three-node network motifs annotated in
698 the GRNs. ii) Top one-hundred recurrent TFs within the three-node network motifs.
699 **Supplementary Table 16:** GEBVs and BLUPs of the elected Ames diversity lines.
700 **Supplementary Table 17:** Pearson correlations of phenotypic traits: Growing degree days to
701 silking (GDD_DTS), Growing degree days to anthesis (GDD_DTA), Predicted GEBV of Tassel
702 Branch Number (TBN predicted), Predicted GEBV of Leaf Angle (LA predicted); Predicted
703 GEBV of the three principal components of LA, TBN, and ERN (PhPC1 predicted, PhPC2
704 predicted, PhPC3 predicted),TBN, LA, PhPC1, PhPC2.
705 **Supplementary Table 18:** i) Module-trait correlation of the sixteen modules identified in the
706 comprehensive GCN. ii) maize genes grouped based on the comprehensive GCN modules.
707 **Supplementary Table 19:** Gene co-expression module heritabilities (h2) for leaf angle (LA) and
708 tassel branch number (TBN).
709 **Supplementary Table 20:** GWAS SNP-trait associations for LA, TBN, PhPC1 and PhPC2 from
710 the single-trait approach using two sets of markers.

Supplementary Table 21: GO terms associated with genes proximal to significant SNP-trait associations from the single-trait GWAS for PhPC2.

Supplementary Table 22: Multi-trait GWAS SNP-trait associations for LA, TBN using two sets of markers.

Supplementary Table 23: Predicted direct gene targets of EREB184 and ZHD21 in the 'leaf' GRN.

Supplementary Table 24: Statistical genetic interaction predictions between *ereb184 and* top recurrent TFs within three-node network motifs.

Supplementary Table 25: Single-trait GWAS results for LA based markers subset around sorghum orthologs of the highly connected three-node motifs in the maize networks.

Supplementary Table 26: GO terms associated with genes in position Z of *ereb184*-controlled FFLs in the 'leaf' network.

Data accessibility

Raw and processed data are available through NCBI Gene Expression Omnibus (GEO) database using the identification number GSE180593.

The manuscript utilizes data from various public datasets, including: conserved non-coding sequences [44] and unmethylated regions [43], which were downloaded from https://www.maizegdb.org, tassel inflorescence ATAC-seq and tassel chromatin interaction (Hi-C) (SRA ID: SRR10873334, SRR10873333, SRR10873339, SRR10873340, SRR10873341, SRR10873342, SRR10873343) [41], leaf chromatin interaction data (Hi-C) (SRA ID: SRR7889833, SRR7889834) [42].

Acknowledgements

The authors would like to thank members of the Eveland, Lipka and Hake labs who assisted in tissue dissections and/or field phenotyping that contributed to this manuscript, namely Dr. Annis Richardson, Dr. Rajiv Parvathaneni, Dr. Samuel Leiboff, Dr. Matthew Murphy, Dr. Indrajit Kumar, Dr. Samuel Bonfim Fernandes, Ms. Zhonghui Wang, Ms. Adrianna Chepote, Dr. Yuguo Xiao, and Mr. Jake Sinkowitz. Also, a dear thanks to Dr. Todd Mockler and members of his team, Mr. Robert Lowery, Mr. Darren O'Brian, and Mr. Phil Ozersky, for their assistance in field phenotyping. We also thank Dr. Baoxing Song and Dr. M. Cinta Romay for providing the AGPv4 genome alignment BAM files for the resequencing data of the Maize 282 Association Panel.

A special thank you to Kevin Reilly and his team in the Danforth Center Integrated Plant Growth Facility for their help with plant care as well as Noah Fahlgren and his team in the Danforth Data Science Core Facility with maintaining computational infrastructure used for this project.
This work was funded by a National Science Foundation Plant Genome Research Project award # IOS-1733606 to ALE, AEL and SH.

Authors' contributions

ALE, AEL and SH designed the research. EB performed network analyses, data integration and interpretation. BRR performed genotype selection and multi-trait GWAS. MB and JY contributed to experimental design and performed molecular and genetics experiments. EB and JS performed genetic analyses of *zhd* alleles, EB and ALE wrote the paper with input from all authors. All authors contributed to editing the final manuscript, read and approved the final manuscript.

References

1. Doebley, J. F., Gaut, B. S. & Smith, B. D. The molecular genetics of crop domestication. *Cell* **127**, 1309–1321 (2006).
2. Abraham-Juárez, M. J. *et al.* The arches and spandrels of maize domestication, adaptation, and improvement. *Curr. Opin. Plant Biol.* **64**, 102124 (2021).
3. Duncan, W. G., Williams, W. A. & Loomis, R. S. Tassels and the productivity of maize 1. *Crop Sci.* **7**, 37–39 (1967).
4. Duvick, D. N. GENETIC PROGRESS IN YIELD OF UNITED STATES MAIZE (Zea mays L.). *Maydica* **50**, 193–202 (2005).
5. Tian, J. *et al.* Teosinte ligule allele narrows plant architecture and enhances high-density maize yields. *Science* **365**, 658–664 (2019).
6. Wang, B. *et al.* Genome-wide selection and genetic improvement during modern maize breeding. *Nat. Genet.* **52**, 565–571 (2020).
7. Gaarslev, N., Swinnen, G. & Soyk, S. Meristem transitions and plant architecture—learning from domestication for crop breeding. *Plant Physiol.* **187**, 1045–1056 (2021).

774 8. Whipple, C. J. Grass inflorescence architecture and evolution: the origin of novel signaling
775 centers. *New Phytol.* **216**, 367–372 (2017).
776 9. Richardson, A. E. & Hake, S. Drawing a Line: Grasses and Boundaries. *Plants* **8**, (2018).
777 10. Johnston, R. *et al.* Transcriptomic analyses indicate that maize ligule development
778 recapitulates gene expression patterns that occur during lateral organ initiation. *Plant Cell*
779 **26**, 4718–4732 (2014).
780 11. Eveland, A. L. *et al.* Regulatory modules controlling maize inflorescence architecture.
781 *Genome Res.* **24**, 431–443 (2014).
782 12. Moreno, M. A., Harper, L. C., Krueger, R. W., Dellaporta, S. L. & Freeling, M. liguleless1
783 encodes a nuclear-localized protein required for induction of ligules and auricles during
784 maize leaf organogenesis. *Genes Dev.* **11**, 616–628 (1997).
785 13. Walsh, J., Waters, C. A. & Freeling, M. The maize gene liguleless2 encodes a basic leucine
786 zipper protein involved in the establishment of the leaf blade-sheath boundary. *Genes Dev.*
787 **12**, 208–218 (1998).
788 14. Walsh, J. & Freeling, M. The liguleless2 gene of maize functions during the transition from
789 the vegetative to the reproductive shoot apex. *Plant J.* **19**, 489–495 (1999).
790 15. Lewis, M. W. *et al.* Gene regulatory interactions at lateral organ boundaries in maize.
791 *Development* **141**, 4590–4597 (2014).
792 16. Kir, G. *et al.* RNA Interference Knockdown of BRASSINOSTEROID INSENSITIVE1 in
793 Maize Reveals Novel Functions for Brassinosteroid Signaling in Controlling Plant
794 Architecture. *Plant Physiol.* **169**, 826–839 (2015).
795 17. Nolan, T. M., Vukašinović, N., Liu, D., Russinova, E. & Yin, Y. Brassinosteroids:
796 Multidimensional Regulators of Plant Growth, Development, and Stress Responses. *Plant*
797 *Cell* **32**, 295–318 (2020).
798 18. Carroll, S. B. Evo-devo and an expanding evolutionary synthesis: a genetic theory of
799 morphological evolution. *Cell* **134**, 25–36 (2008).

800 19. Brown, P. J. *et al.* Distinct genetic architectures for male and female inflorescence traits of
801 maize. *PLoS Genet.* **7**, e1002383 (2011).
802 20. Carroll, S. B. Evolution at two levels: on genes and form. *PLoS Biol.* **3**, e245 (2005).
803 21. Marand, A. P., Eveland, A. L., Kaufmann, K. & Springer, N. M. cis-Regulatory Elements in
804 Plant Development, Adaptation, and Evolution. *Annu. Rev. Plant Biol.* **74**, 111–137 (2023).
805 22. Song, X. *et al.* Targeting a gene regulatory element enhances rice grain yield by decoupling
806 panicle number and size. *Nat. Biotechnol.* (2022) doi:10.1038/s41587-022-01281-7.
807 23. Hendelman, A. *et al.* Conserved pleiotropy of an ancient plant homeobox gene uncovered
808 by cis-regulatory dissection. *Cell* **184**, 1724–1739.e16 (2021).
809 24. Bell, E. M. *et al.* Arabidopsis lateral organ boundaries negatively regulates brassinosteroid
810 accumulation to limit growth in organ boundaries. *Proc. Natl. Acad. Sci. U. S. A.* **109**,
811 21146–21151 (2012).
812 25. Gendron, J. M. *et al.* Brassinosteroids regulate organ boundary formation in the shoot
813 apical meristem of Arabidopsis. *Proc. Natl. Acad. Sci. U. S. A.* **109**, 21152–21157 (2012).
814 26. Chuck, G. S., Brown, P. J., Meeley, R. & Hake, S. Maize SBP-box transcription factors
815 unbranched2 and unbranched3 affect yield traits by regulating the rate of lateral primordia
816 initiation. *Proc. Natl. Acad. Sci. U. S. A.* **111**, 18775–18780 (2014).
817 27. Kellogg, E. A. Genetic control of branching patterns in grass inflorescences. *Plant Cell* **34**,
818 2518–2533 (2022).
819 28. Langfelder, P. & Horvath, S. Eigengene networks for studying the relationships between co-
820 expression modules. *BMC Syst. Biol.* **1**, 54 (2007).
821 29. Bolduc, N. *et al.* Unraveling the KNOTTED1 regulatory network in maize meristems. *Genes*
822 *Dev.* **26**, 1685–1690 (2012).
823 30. Xiao, Y. *et al.* Boundary domain genes were recruited to suppress bract growth and
824 promote branching in maize. *Sci Adv* **8**, eabm6835 (2022).
825 31. Leiboff, S. *et al.* Network analyses identify a transcriptomic proximodistal prepattern in the

826 maize leaf primordium. *New Phytol.* (2020) doi:10.1111/nph.17132.
827 32. Milo, R. *et al.* Network motifs: simple building blocks of complex networks. *Science* **298**,
828 824–827 (2002).
829 33. Alon, U. Network motifs: theory and experimental approaches. *Nat. Rev. Genet.* **8**, 450–461
830 (2007).
831 34. Flint-Garcia, S. A. *et al.* Maize association population: a high-resolution platform for
832 quantitative trait locus dissection. *Plant J.* **44**, 1054–1064 (2005).
833 35. Romay, M. C. *et al.* Comprehensive genotyping of the USA national maize inbred seed
834 bank. *Genome Biol.* **14**, R55 (2013).
835 36. Peiffer, J. A. *et al.* The genetic architecture of maize height. *Genetics* **196**, 1337–1356
836 (2014).
837 37. Liu, W.-Y. *et al.* Maize ANT1 modulates vascular development, chloroplast development,
838 photosynthesis, and plant growth. *Proc. Natl. Acad. Sci. U. S. A.* **117**, 21747–21756 (2020).
839 38. McSteen, P. *et al.* barren inflorescence2 Encodes a co-ortholog of the PINOID
840 serine/threonine kinase and is required for organogenesis during inflorescence and
841 vegetative development in maize. *Plant Physiol.* **144**, 1000–1011 (2007).
842 39. Casa, A. M. *et al.* Community resources and strategies for association mapping in
843 sorghum. *Crop Sci.* **48**, 30–40 (2008).
844 40. Mantilla Perez, M. B., Zhao, J., Yin, Y., Hu, J. & Salas Fernandez, M. G. Association
845 mapping of brassinosteroid candidate genes and plant architecture in a diverse panel of
846 Sorghum bicolor. *Theor. Appl. Genet.* **127**, 2645–2662 (2014).
847 41. Sun, Y. *et al.* 3D genome architecture coordinates trans and cis regulation of differentially
848 expressed ear and tassel genes in maize. *Genome Biol.* **21**, 143 (2020).
849 42. Ricci, W. A. *et al.* Widespread long-range cis-regulatory elements in the maize genome.
850 *Nat Plants* (2019) doi:10.1038/s41477-019-0547-0.
851 43. Hufford, M. B. *et al.* De novo assembly, annotation, and comparative analysis of 26 diverse

852 maize genomes. *Science* **373**, 655–662 (2021).

853 44. Song, B. *et al.* Conserved noncoding sequences provide insights into regulatory sequence
854 and loss of gene expression in maize. *Genome Res.* **31**, 1245–1257 (2021).

855 45. Grassini, P., Eskridge, K. M. & Cassman, K. G. Distinguishing between yield advances and
856 yield plateaus in historical crop production trends. *Nat. Commun.* **4**, 2918 (2013).

857 46. Bailey-Serres, J., Parker, J. E., Ainsworth, E. A., Oldroyd, G. E. D. & Schroeder, J. I.
858 Genetic strategies for improving crop yields. *Nature* **575**, 109–118 (2019).

859 47. Eshed, Y. & Lippman, Z. B. Revolutions in agriculture chart a course for targeted breeding
860 of old and new crops. *Science* **366**, (2019).

861 48. Lipka, A. E. *et al.* Genome-wide association study and pathway-level analysis of
862 tocochromanol levels in maize grain. *G3* **3**, 1287–1299 (2013).

863 49. Parvathaneni, R. K. *et al.* The regulatory landscape of early maize inflorescence
864 development. *Genome Biol.* **21**, 165 (2020).

865
866
867

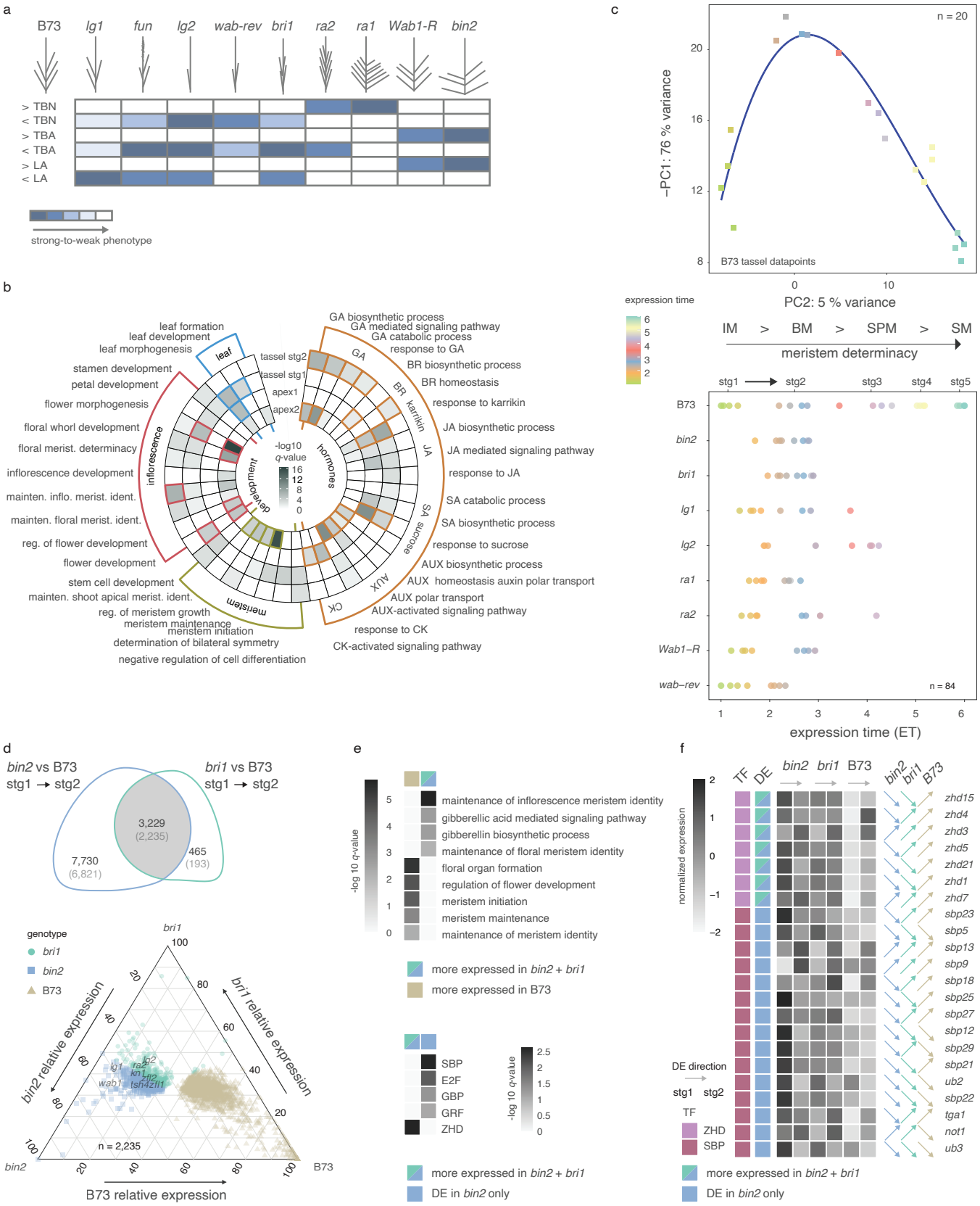

Fig.1: Transcriptional analyses across maize mutants with defects in leaf angle and tassel branching
a) Panel of maize mutants used in this study depicting unique tassel branching phenotypes compared to B73 controls. Color scale in the heatmap indicates severity of tassel branch number (TBN), tassel branch angle (TBA) and leaf angle (LA) phenotype deviations from B73 controls; dark blue-to-white = strong-to-weak phenotype. **b)** Enrichment of GO terms associated with DE gene sets identified during the shift from stage (stg) 1 to stg 2 tassel primordia and from shoot apex 1 to shoot apex 2. **c)** A 2-dimensional section of the first and second PC from ...

Fig.1... the normal B73 tassel developmental gradient (n = 20). The blue line represents the b-spline fit with three degrees of freedom modeled within the dataset and used to classify samples relative to their developmental progression coded as expression time (ET). Colored squares represent the 20 tassel samples in ET. The dot plot below represents tassel primordia stgs 1 and 2 from the different mutant backgrounds. Mutant data points are color-coded relative to B73 ET. Stages of meristem development along normal tassel developmental time are indicated: inflorescence meristem (IM), branch meristem (BM), spikelet pair meristem (SPM), spikelet meristem (SM). **d**) Venn diagram shows genes that are DE in tassel primordia during shift from stg 1 to 2 and DE in *bri1-RNAi* and *bin2-RNAi* mutants compared to B73 controls. Those with stronger deviations at stg1 are shown in parentheses. The ternary plot below shows the relative expression of genes commonly mis-expressed between the two mutants compared to B73 at stg 1. Each dot represents a gene and its coordinates indicate relative expression in the three genotypes. Some examples of classical maize genes are noted. **e**) The top heatmap shows GO terms enriched among DE gene sets commonly expressed either higher or lower in the BR mutants compared to B73 controls in stg 1 tassels (from the ternary plot in d); the bottom heatmap shows overrepresented TF classes among genes expressed higher in bri1 and bin2 mutants at stg 1 and those expressed higher in bin2 only compared to B73 controls. **f**) Relative gene expression trends are shown for ZHD and SBP TF family members that were expressed higher in bin2 and/or bri1 mutants compared to B73 controls at stg 1. Arrows indicate direction of expression change between stg 1 and 2 tassel primordia.

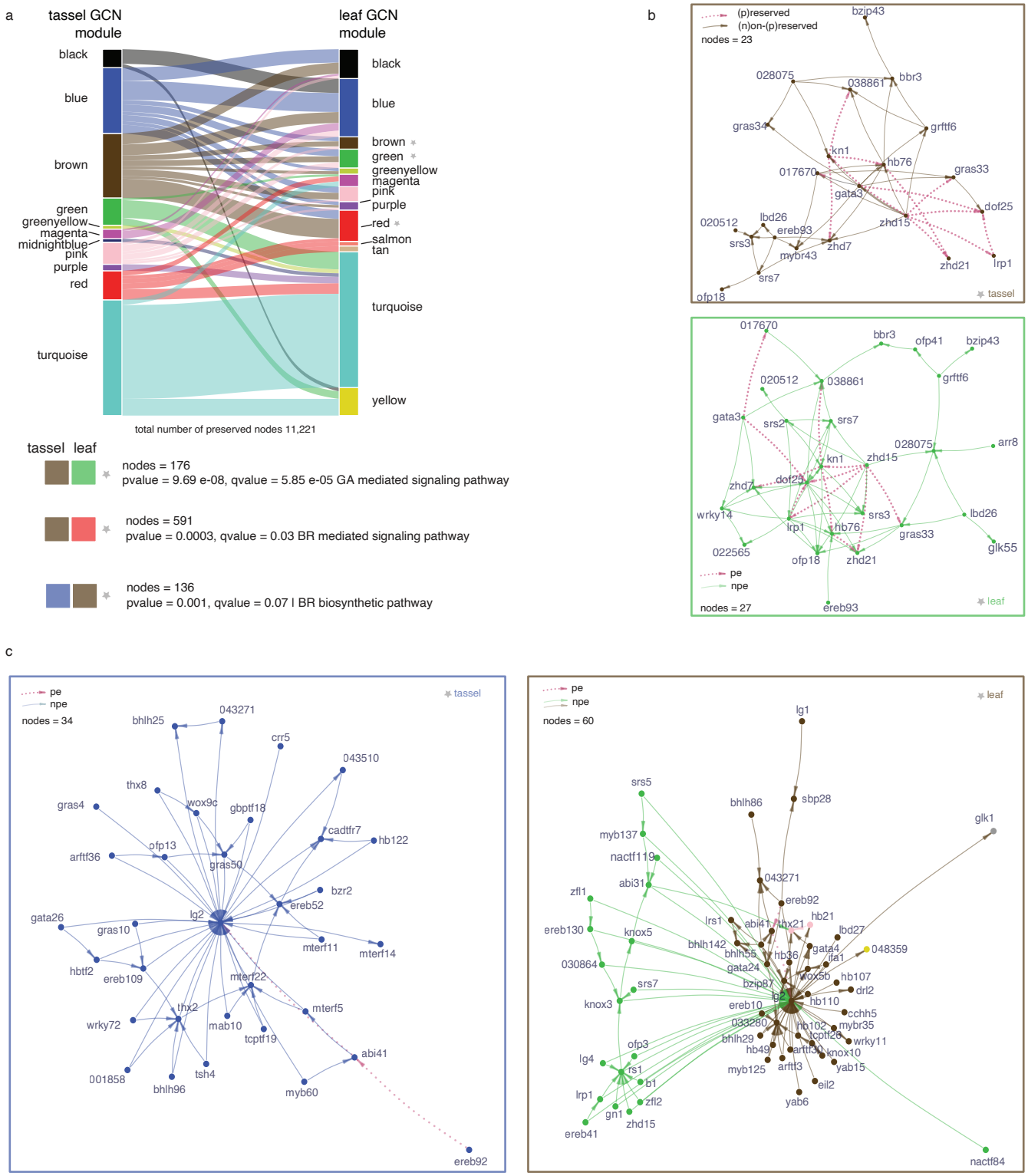

Fig.2: Conserved and divergent network connections between tassel and leaf gene regulatory networks
a) Gene co-expression network (GCN) preservation between 'tassel' and 'leaf' networks. Preserved modules are indicated by color and connected by lines (width is proportional to number of preserved genes). Colored boxes beneath the plot represent example preserved gene co-expression sub-modules. **b**) Topological graph representation of preserved TFs in the 'tassel'-'leaf' "brown-green" sub-module based on data from GCN (edge weight) and gene regulatory network (GRN; edge directionality). Pink edges represent preserved regulatory connections and brown or green edges represent the network-specific wires. c) Topological graph representation of closest TF neighbors to *liguleless2* (*lg2*) in the 'tassel' and 'leaf' networks based on data from GCN (edge weight) and GRN (edge directionality). Pink edges represent preserved connections and blue or brown/green edges represent network-specific wires. The edge length is proportional to the weight of gene co-expression. Nodes are colored based on ...

Fig.2:... their GCN module designation. Maize gene labels are from MaizeGDB or AGPv4 as Zm00001d$_{(6)}$.

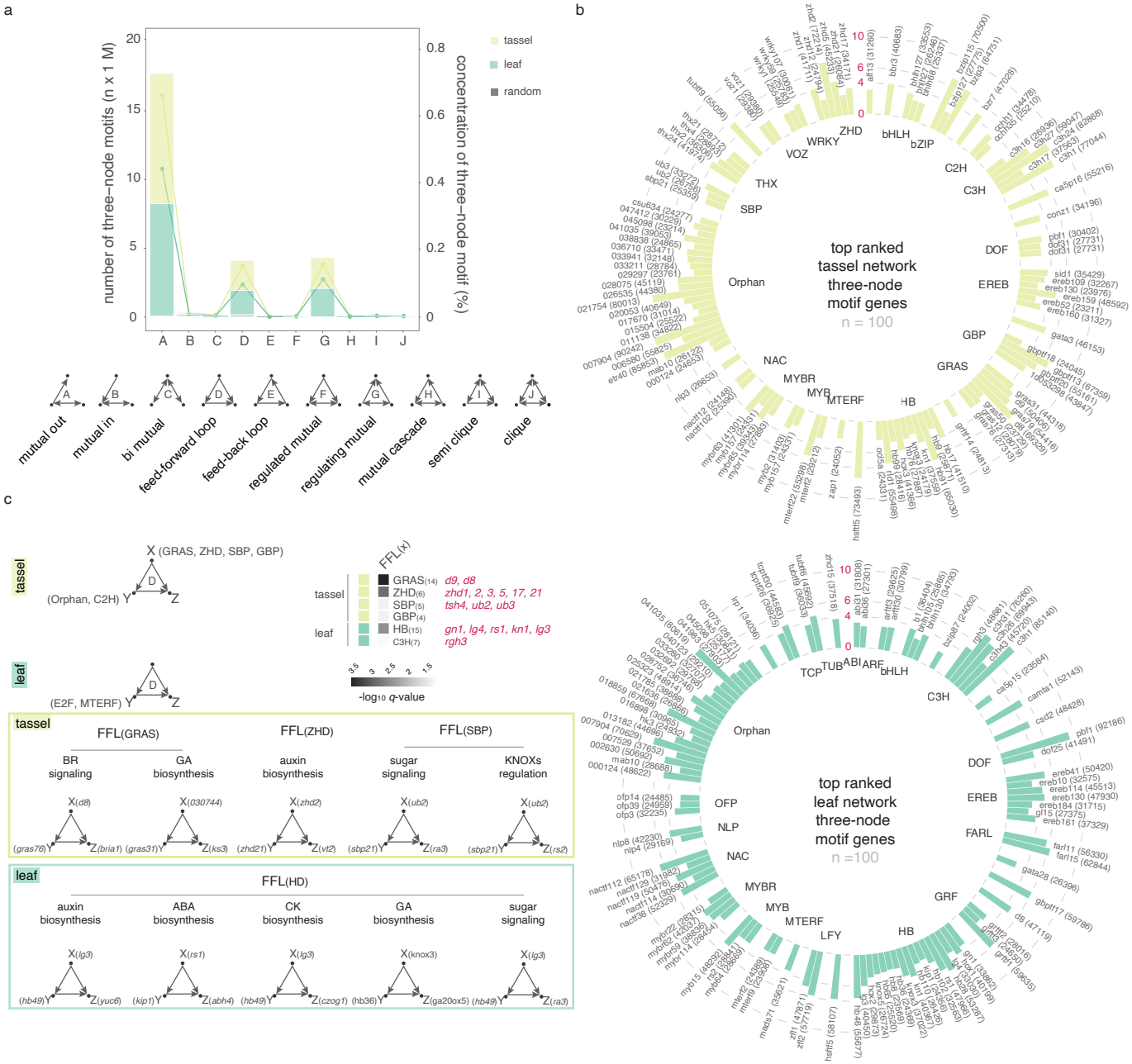

Fig.3: Analysis of three-node network motifs

a) The number and type of three-node motifs identified in 'tassel' and 'leaf' networks compared to randomized networks (*n*=1,000). The x-axis represents the motif type (from A to J) of three-node motifs with edge number ≥ 3. **b**) Top 100 ranked TFs based on their occurrence in the three-node motifs grouped by family. Bars represent TF frequency in the three-node motif (scale in red is TF frequency / 10,000); non-normalized values are within parentheses. TF labels are from MaizeGDB or AGPv4 as Zm00001d$_{(6)}$. **c**) Examples of feed-forward loop (FFL) motifs mediated by select TFs. The heatmap displays overrepresented TFs in FFL$_{(X)}$, (examples of genes in each TF family are noted). Nodes represent genes, while the directed edges represent the potential regulatory relationships.

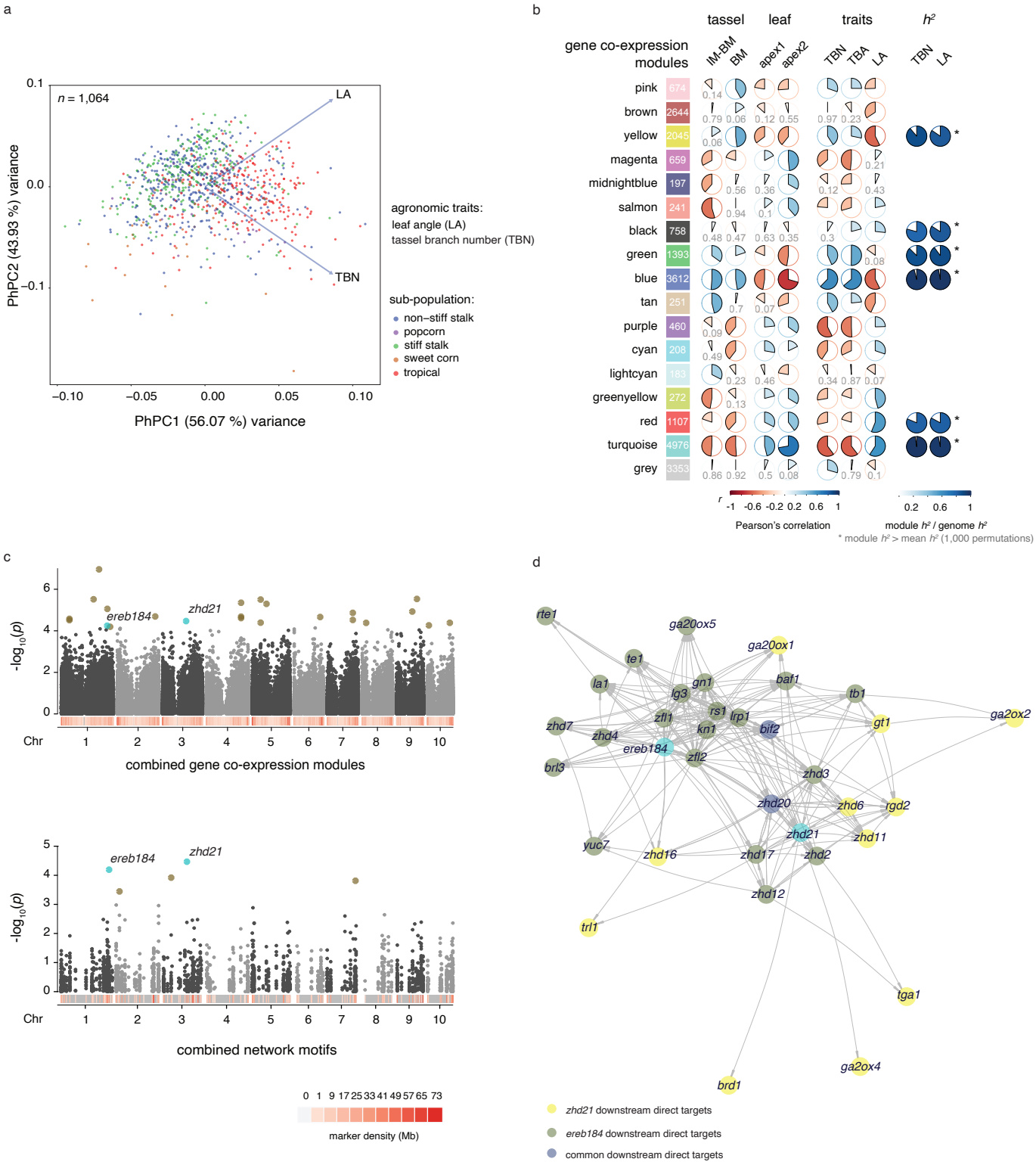

Fig.4: Multi-trait GWAS detected candidate pleiotropic genes for TBN and LA

a) Phenotypic Principal Components (PhPCs) of TBN and LA. Individuals are plotted according to their PhPC1 scores of TBN and LA on the x-axis and their PhPC2 scores on the y-axis. The percentage of total variance explained by a component is listed in parentheses on the axis. Blue arrows represent trait loadings for a given PhPC where its direction on the x-axis represents its contribution to PhPC1 and direction on the y-axis, its contribution to PhPC2. Subpopulations are color-coded and grouped according to PhPCs. **b**) Analysis of module-trait relationships for the combined GCN. Modules are represented as colored boxes with the number of co-expressed genes indicated. The correlogram to the right represents the module-trait relationship where shades of blue and red represent positive and negative Pearson's correlation, respectively, with darker color indicating a stronger positive or negative correlation. Modules representing more than 80% of the whole genome heritability (h^2) for TBN and LA are ...

Fig.4:... indicated. **c**) Multi-trait GWAS results using subsets of markers within 2 kb proximity of genes in the six co-expression modules with significant h^2 in panel b (top) and in the top 200 interconnected TFs within three-node motifs from Fig. 3b. Brown and blue dots represent significant SNP-trait associations; blue dots indicate loci identified in both analyses. **d**) Topological graph representation of a sub-network including *ereb184*, *zhd21* and their predicted downstream target genes based on data from the 'leaf' GRN (edge directionality).

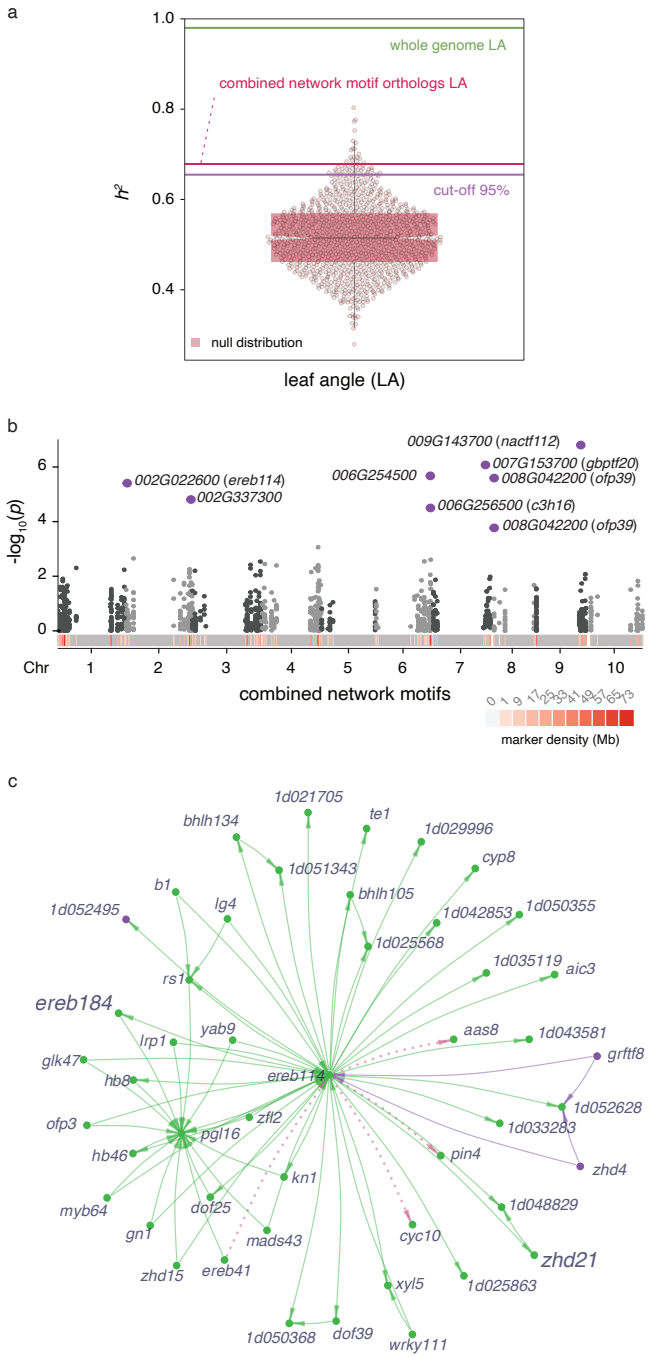

Fig.5: GWAS for LA in sorghum using biological information derived from maize.
a) LA narrow-sense heritability of 146 sorghum-maize syntenic orthologs in comparison to a null distribution (violin plot). Purple line represents 95% cut-off, red line represents LA h^2 of the sorghum orthologs, green line is the whole genome LA h^2. **b**) Manhattan plot showing GWAS results for LA based on markers in proximity of the 146 sorghum-maize syntenic orthologs. Purple dots represent significant SNP-trait associations for LA. **c**) Topological graph representation of *ereb114* and its closest network neighbors in the maize 'leaf' GCN (edge weight) and GRN (edge directionality). Green and purple nodes and edges are colored based on module assignment in the 'leaf' GCN. Pink edges represent preserved connections with the 'tassel' GCN. Edge length is proportional with the gene co-expression weight.

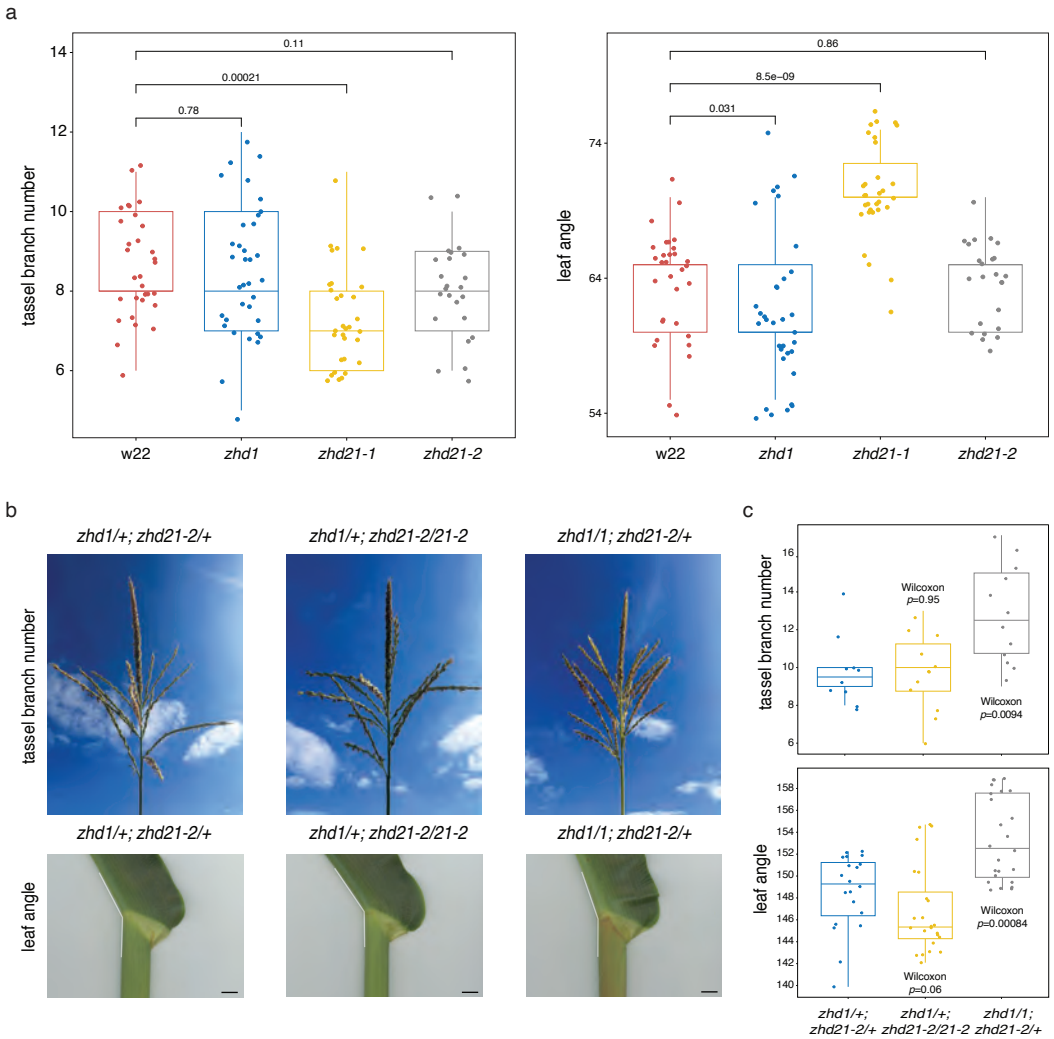

Fig. 6: *zhd* mutant alleles contribute to tassel and leaf architecture.
a) Phenotypic characterization of TBN and LA in homozygous *zhd* alleles compared with w22 control plants. **b**) Representative tassel branch and leaf angle phenotypes resulting from genetic interactions between mutant alleles of *zhd1* and *zhd21*, from left to right: *zhd1/+;zhd21-2/+*, *zhd1/+;zhd21-2/zhd21-2*, *zhd1/1;zhd21-2/+*. Black bar = 1cm. **c**) Among combinations of mutant alleles, *zhd1/1;zhd21-2/+* showed significant differences in TBN and LA compared to *zhd1/+;zhd21-2/+* normal siblings based on Wilcoxon rank-sum test.

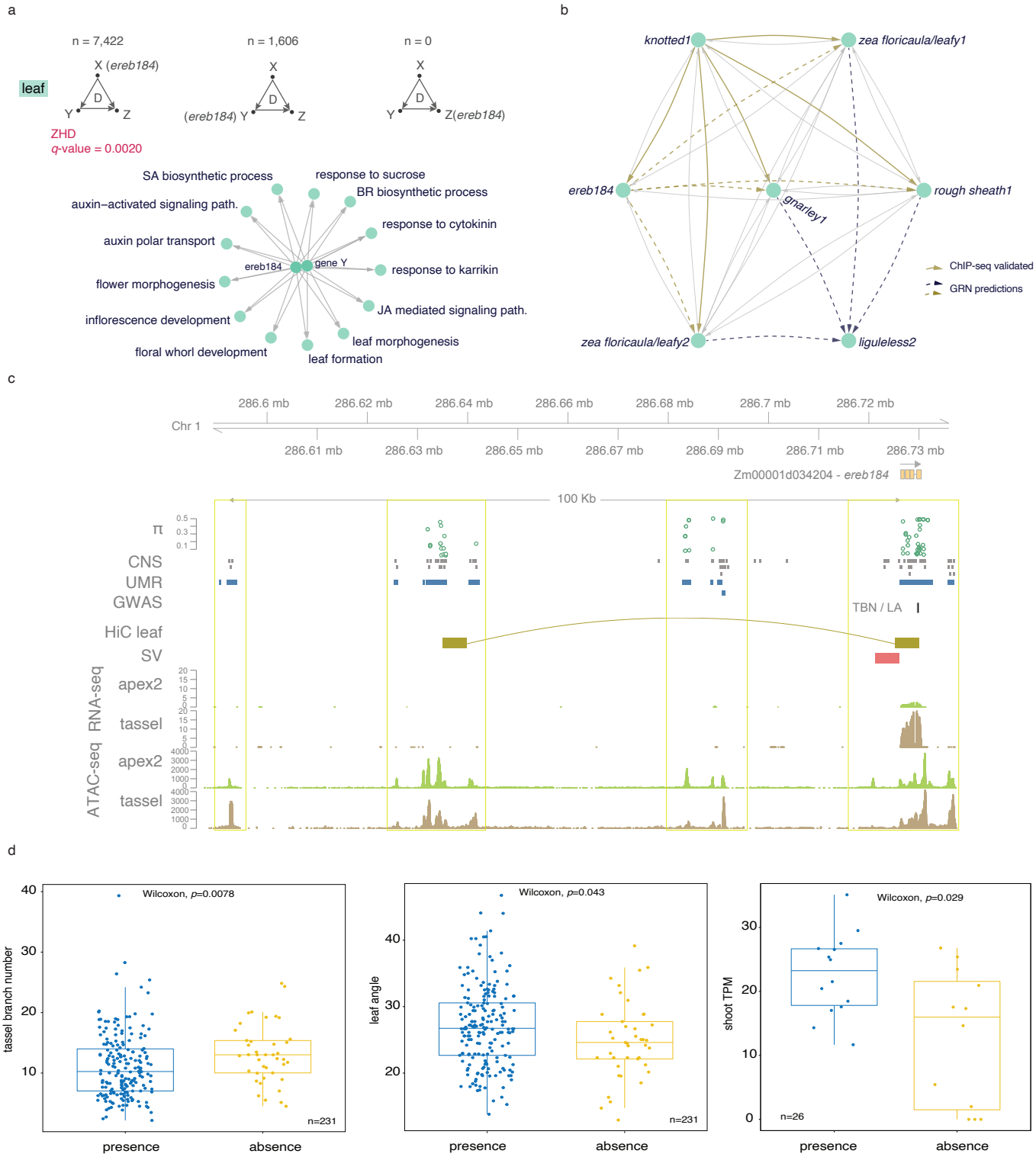

Fig.7: *ereb184* modulates pleiotropy in TBN and LA

a) FFLs from the 'leaf' GRN are represented with *ereb184* in each of the node positions and number of times each occurs. The graph below shows GO terms overrepresented within the Z position when EREB184 is in the X position. **b**) An example of a sub-network from the 'leaf' GRN shows *ereb184* participating in multiple FFLs with KN1 and other proximal-distal patterning TFs that target *lg2*. The solid yellow arrows represent ChIP-seq validated connections. **c**) Genomic view of the intergenic space upstream (100 kb) and just downstream of ereb184. The tracks from top to bottom: nucleotide diversity (π), conserved non-coding sequences, multi-trait GWAS, unmethylated regions, leaf chromatin interaction data (Hi-C), structural variation, RNA-seq, and ATAC-seq. Data from public sources are indicated in Data Accessibility. **d**) The effect of structural variation (SV) presence/absence in the promoter region of *ereb184* across 231 accessions on TBN and LA traits, and the effect of SV on *ereb184* expression within 26 NAM founder lines.